



**HAL**  
open science

## Electrical, dielectric, and optical properties of Sb<sub>2</sub>O<sub>3</sub>–Li<sub>2</sub>O–MoO<sub>3</sub> glasses

Marian Kubliha, M. T. Soltani, V. Trnovcová, M. Legouera, Vladimir Labaš,  
Petr Kostka, David Le Coq, Majda Hamzaoui

► **To cite this version:**

Marian Kubliha, M. T. Soltani, V. Trnovcová, M. Legouera, Vladimir Labaš, et al.. Electrical, dielectric, and optical properties of Sb<sub>2</sub>O<sub>3</sub>–Li<sub>2</sub>O–MoO<sub>3</sub> glasses. *Journal of Non-Crystalline Solids*, 2015, 428, pp.42–48. 10.1016/j.jnoncrysol.2015.07.021 . hal-01202035

**HAL Id: hal-01202035**

**<https://univ-rennes.hal.science/hal-01202035>**

Submitted on 20 Oct 2015

**HAL** is a multi-disciplinary open access archive for the deposit and dissemination of scientific research documents, whether they are published or not. The documents may come from teaching and research institutions in France or abroad, or from public or private research centers.

L'archive ouverte pluridisciplinaire **HAL**, est destinée au dépôt et à la diffusion de documents scientifiques de niveau recherche, publiés ou non, émanant des établissements d'enseignement et de recherche français ou étrangers, des laboratoires publics ou privés.

# Electrical, dielectric, and optical properties of $\text{Sb}_2\text{O}_3\text{-Li}_2\text{O-MoO}_3$ glasses

M. Kubliha<sup>1</sup>, M. T. Soltani<sup>2</sup>, V. Trnovcová<sup>3</sup>, M. Legouera<sup>4</sup>, V. Labaš<sup>5</sup>, P. Kostka<sup>6</sup>, D. Le Coq<sup>7</sup>,  
M. Hamzaoui<sup>2</sup>

<sup>1</sup>*Faculty of Civil Engineering, Slovak University of Technology, Radlinského 11, Bratislava,  
Slovakia,*

*marian.kubliha@stuba.sk*

<sup>2</sup>*Laboratoire de physique photonique et nanomatériaux multifonctionnels, University of Biskra, BP  
145, Biskra, Algeria*

*mt.soltani@univ-biskra.dz, hamzaouimajda@yahoo.fr*

<sup>3</sup>*Faculty of Natural Sciences, Constantine the Philosopher University, A. Hlinku 1, 949 74 Nitra,  
Slovakia,*

*trnovcovaviera@gmail.com*,

<sup>4</sup>*Laboratoire de Génie Mécanique et Matériaux, Université de Skikda, 21000 Algérie,*

*legouira@yahoo.fr*,

<sup>5</sup>*Faculty of Materials Science and Technology, Slovak University of Technology, Trnava, Slovakia,*

*vladimir.labas@stuba.sk*,

<sup>6</sup>*Institute of Rock Structure and Mechanics, Czech Academy of Sciences, Czech Republic,*

*petr.kostka@irsm.cas.cz*,

<sup>7</sup>*University of Rennes 1 – Institute of Chemical Sciences of Rennes, France,*

*david.lecoq@univ-rennes1.fr*.

## Abstract

Temperature and frequency dependencies of DC and AC conductivities, dielectric response, static permittivity, optical absorption edge, infrared absorption spectrum, density, and temperatures of glass transition and crystallization for lithium molybdenum-antimonite glasses,  $(80-x)\text{Sb}_2\text{O}_3\text{-}20\text{Li}_2\text{O-xMoO}_3$ , where  $x = 0 - 40$ , are measured and discussed. The DC conductivity increases with increasing concentration

of MoO<sub>3</sub>. At 150°C, it ranges from 5x10<sup>-11</sup> S/m up to 3x10<sup>-8</sup> S/m. Polaron hopping between Mo<sup>5+</sup> and Mo<sup>6+</sup> ions contributes, probably, to the DC conductivity. Ionic conductivity by Li<sup>+</sup> ions is also present. The conduction activation energy monotonously decreases from 1.15 eV, at  $x = 5$ , down to 0.91eV, at  $x = 40$ . In all glasses with  $x > 0$ , the conduction activation energy is close to a half of the indirect allowed optical gap. The pre-exponential factor,  $\sigma_0$ , goes through a sharp maximum close to the composition ( $x = 20$ ) with both the highest glass transition temperature and the largest thermal stability range. The frequency dependence of the AC conductivity is composed of three components – the DC conductivity and two AC components. For  $x = 35$  and 40, the activation energy of electrical relaxation is equal to 0.954±0.008 eV and the pre-exponential factor of relaxation times is equal to (4±1)·10<sup>-14</sup> s. The static relative permittivity ranges from 17.4 to 23.0. Strong extrinsic absorption bands in infrared region originate from hydroxyl ions, CO<sub>2</sub> impurities, and silicon-oxygen vibrations. The UV-visible indirect allowed absorption edge shifts from 2.6 eV to 2.1 eV with increasing MoO<sub>3</sub> content. With increasing MoO<sub>3</sub> content the glasses darken, from a light yellow color, at  $x = 0$ , to a deep brown color, at  $x = 40$ .

**PACS:** 72.80.Ng, 77.22.Ch, 78.30.-j, 78.40-q

**Keywords:** lithium molybdenum-antimonite glasses, electrical conductivity, electrical relaxation, dielectric response, optical properties.

\*Corresponding author. Tel.: +421 904046260, fax +421 2 5296 7027.

*E-mail address:* marian.kubliha@stuba.sk

## 1. Introduction

Antimonite glasses form a major and important family of heavy metal oxide glasses [1-5]. They are attractive for their low phonon energy, broad transmission spectrum, and high refractive index. Their broad thermal stability range appears promising for fiber drawing [3]. They have potential applications in non-linear optical devices and in broad band optical amplifiers. The large nonlinearity of antimonite glasses is attributed to the high polarizability of Sb<sup>3+</sup> ions due to contributions from the bound electrons and lone electron pairs [6, 7]. Sb<sub>2</sub>O<sub>3</sub> is a heavy metal oxide glass former with a relatively low liquidus temperature [1, 2]. An increase of the thermal stability and resistance against crystallization can be achieved by adding

MoO<sub>3</sub> in the glass matrix [1]. It exhibits also some glassforming ability in multicomponent systems. Alkali metal oxides, e.g. Li<sub>2</sub>O, are added to enlarge the glassforming region and to enhance the stability of the glass [1, 2].

Antimony oxide participates in the glass network with trigonal pyramidal [SbO<sub>3</sub>] structural units sharing corners which can be viewed as tetrahedrons with the oxygen at three corners and a lone pair of electrons at the fourth corner [8-9]. Such structural unit can be also considered as pseudo-tetrahedral unit with one vertex occupied by the lone pair of electrons [8]. Antimony ions exist not only in the Sb<sup>3+</sup> state but also in the Sb<sup>5+</sup> oxidation state. In the Sb<sup>5+</sup> state, ions participate in the glass network as octahedral [SbO<sub>6</sub>] units [8] or as singly positive [Sb<sup>5+</sup>O<sub>4</sub>]<sup>+</sup>, 4-coordinated structural units [10, 11]. The MoO<sub>3</sub>→Sb<sub>2</sub>O<sub>3</sub> substitution brings an excess of anionic oxygen which increases the number of non-bridging oxygen [9, 12]. Molybdenum ions exist in two states as Mo<sup>5+</sup> and Mo<sup>6+</sup> [10]. Mo<sup>6+</sup> ions participate in the glass network with [MoO<sub>4</sub>] tetrahedrons; in MoO<sub>3</sub>-rich region, [MoO<sub>6</sub>] octahedrons are also present. These octahedrons are linked to [MoO<sub>4</sub>] tetrahedrons via bridging oxygen and in this way they increase the network connectivity [12]. The Mo<sup>6+</sup> ions act as network formers with [MoO<sub>4</sub>]<sup>2-</sup> structural units [13-15]; the Mo<sup>5+</sup> ions form [Mo<sup>5+</sup>O<sub>3</sub>]<sup>-</sup> complexes which act as network modifiers [12].

Last years an intensive attention was given to antimonite glasses because of their similar physical properties to widely used tellurite glasses without specific problems related to tellurium toxicity [1-10, 16-18]. They have a broad thermal stability range and so they are also suitable for fiber drawing [3]. This paper deals with the new glassy system Sb<sub>2</sub>O<sub>3</sub>-MoO<sub>3</sub>-Li<sub>2</sub>O. This system represents an interesting combination of glass-forming, intermediate, and modifying oxides. Only few papers dealing with this system appeared up to now. These papers were dealing with absorption spectra in the Urbach's rule region [19], FTIR spectra, elastic properties, and some basic parameters of this system [20]. However, the system is also interesting from the point of view of its electrical conduction and relaxation as it represents a mixed ionic-polaronic conductor. Therefore, we have studied the influence of composition on its thermal, electrical, dielectric, and optical properties and we also examined relations between the composition, glass structure, and these properties.

## 2. Experimental

The starting composition used in this study is a ternary system:  $(80-x)\text{Sb}_2\text{O}_3-20\text{Li}_2\text{O}-x\text{MoO}_3$ ,  $\text{SLM}_x$ , where  $x = 0 - 40$ . Materials used are  $\text{Sb}_2\text{O}_3 \geq 99\%$  (Acros),  $\text{Li}_2\text{O} \simeq 99\%$  (Alfa Aesar), and  $\text{MoO}_3 \simeq 99+\%$  (Acros). Synthesis is carried out in several steps. Batches, around 10 g in weight, are made from thoroughly mixed powders. The mixture is introduced into a silica tube, around 10 mm in diameter and 10 cm in height, and heated by burner flame until a clear liquid is obtained. After that the melt is cast onto a brass plate preheated to approximately 200 °C. Estimated cooling rate ranges from 10 °C/s to 100 °C/s. It results in samples a few millimeters in thickness which are afterwards polished for experimental purposes.

The samples for measurements of electrical and dielectric properties (thickness of  $2.6 \pm 0.3$  mm) are coated with a conductive graphite layer on contact surfaces. DC conductivity is measured at a constant voltage of 10 V using Novocontrol Concept 90, in the temperature range from -50 °C up to 225 °C. The current is measured by picoammeter Keithley 6517B. The temperature is measured using a Pt/PtRh thermocouple, with an accuracy of  $\pm 1$  °C. Temperature dependencies of the DC conductivity are measured at increasing temperature, with a heating rate of 5 °C/min [17]. The combined uncertainty of DC conductivity measurements is equal to 7 % [21].

AC measurements (from 20 °C up to 200 °C) are done using LCR Hi-tester Hioki 3522-50 at frequency range 100 Hz – 100 kHz. Measurements are done in steps of 10 °C, after 20 min's tempering at chosen temperatures. For the evaluation of the bulk DC conductivity the frequency dependence of the AC conductivity is used. To avoid the influence of electrode polarization effects and for better understanding of the electrical relaxation, the modular spectroscopy concept is used [22]. The static relative permittivity is determined using both the modular spectroscopy [9, 10, 22] and Kramers-Kronig relations.

At electrical and dielectric measurements, the temperature or frequency dependences are fitted to the experimental data using Levenberg-Marquardt iteration. Regression coefficients,  $r$ , are given in corresponding tables and figures for all dependences.

The glass composition is analyzed using scanning electron microscope and energy dispersive X-ray spectrometer (SEM-EDS JSM 6400 Jeol and Oxford link ISIS). Crystalline materials are used as standard references. Experimental error depends on the selected element, as signal to noise ratio is smaller for lighter atoms. It is estimated to be 1% for Sb and Mo, 5% for Li and oxygen.

Thermal properties are measured by differential scanning calorimetry (DSC 2010 from TA Instruments) with a heating rate of 10 °C/min. Small bulk samples are used; they are 5 to 10 mg in weight and set in aluminum sealed pans. With sensitivity better than 0.1 °C, the estimated temperature accuracy is  $\pm 2$  °C for the temperatures of glass transition  $T_g$  and onset of crystallization  $T_x$ , and  $\pm 1$  °C for the temperature of the crystallization peak. The difference  $T_x - T_g$ , the thermal stability range, gives an estimate of stability against devitrification.

Micromeritics AccuPyc pycnometer with He as the displacement fluid, with accuracy up to  $\pm 0.05$  % is used to determine the density.

Optical transmission is recorded in the UV-visible region between 250 and 750 nm using Perkin Elmer Lambda 35 device. The optical gap,  $E_g$ , is determined using the Tauc plot. Optical transmission in the infrared region is recorded using Perkin Elmer Spectrum BX device operating between 2.5 and 22  $\mu\text{m}$ .

### 3. Results

Colors of glasses change with increasing  $\text{MoO}_3$  content from light yellow to dark brown (Table 1). This change of the color indicates a partial reduction of  $\text{Mo}^{6+}$  ions to  $\text{Mo}^{5+}$  ions [13]. This reduction results in an increase of the concentration of polaron pairs  $\text{Mo}^{5+}-\text{Mo}^{6+}$ .

The density of glasses decreases with increasing  $\text{MoO}_3$  content due to decreasing molar weight (Table 2). The glass transition temperature,  $T_g$ , the crystallization temperature,  $T_x$ , and the thermal stability range,  $T_x - T_g$ , go through a maximum at 20 mol %  $\text{MoO}_3$  (Table 2, Fig. 1). The large thermal stability range indicates that the glasses can be suitable for a fibre drawing.

Temperature dependences of the DC conductivity,  $\sigma_{\text{DC}}$ , of SLMx glasses are presented in Fig. 2. In the main temperature region (Table 1), the glasses containing  $\text{MoO}_3$  obey Arrhenius like relation

$$\sigma_{\text{DC}} = \sigma_0 \exp(-E_\sigma/kT), \quad (1)$$

where  $\sigma_0$  is the pre-exponential factor,  $E_\sigma$  is the conduction activation energy,  $k$  is Boltzmann constant, and  $T$  is thermodynamic temperature. The DC conductivity increases almost exponentially with increasing concentration of  $\text{MoO}_3$  (Fig. 3). At 150°C, it ranges from  $5 \times 10^{-11}$  S/m up to  $3 \times 10^{-8}$  S/m, in dependence on the concentration of  $\text{MoO}_3$ . For  $x > 0$ , the conduction activation energy monotonously decreases from 1.15 eV, at  $x = 5$ , down to 0.91 eV, at  $x = 40$  (Table 1).

In molybdenum-free glasses, the temperature dependence of the DC conductivity is more complicated (Fig. 2). In these glasses, in both low temperature and high temperature regions, the conduction activation energy decreases to 0.48 eV or 0.78 eV, respectively.

Frequency dependences of the AC conductivity of our glasses are presented in Fig. 4. The dependences are fitted by relation

$$\sigma_{ac}(f) = \sigma(0) + A f^n + B f^m, \quad (2)$$

where  $n = 0.56-0.93$  and  $m \geq 1.6$  (Table 3).

Frequency dependencies of the AC conductivity of the glass SLM25 at various temperatures are presented in Fig. 5. A fit using Eq. (2) gives parameters shown in Table 4. This fit gives parameters  $A$  which increase with increasing temperature and exponents  $n$  decreasing with increasing temperature. Using this fit, we obtain parameters  $\sigma(0)$  which are, in error limits, equal to the DC conductivity at corresponding temperature.

The dielectric response is studied using the modular spectroscopy ( $M^* = M' + jM'' = (\epsilon_r^*)^{-1}$ ) and complex permittivity measurements. The shape of modular diagrams,  $M''$  against  $M'$ , is regular for all our glasses. The diagrams are composed of a slightly depressed circular arc and a high frequency linear tail as it is usual in semiconducting glasses (Figure 6). From modular diagrams, we have calculated relative static permittivity,  $\epsilon_{rs}$ , equal to the reciprocal value of the  $M'$ , which is determined as an intercept of the modular diagram with  $M'$  axis. The calculated values were confirmed by Kramers-Kronig analysis of complex permittivity frequency dependences. The static relative permittivity ( $\epsilon_{rs}$ ) ranges from 17.4 to 23.0 (Table 2). Regular shape of modular spectra (Figure 7) confirms single dominant conduction mechanism and relatively good ordering of glasses. The spectra are broadened comparing to Debye spectra and have high-frequency tail. Their maximums shift to higher frequencies with increasing DC conductivity of glasses; it means that they shift to higher frequencies also with increasing temperature (Fig. 8). From this shift we have calculated the activation energy and pre-exponential factor of the electrical relaxation (Table 5).

UV-visible absorption edge shifts to lower energies and its slope decreases with increasing MoO<sub>3</sub> content (Figure 9). The indirect optical gap,  $E_g$ , shifts from 2.57 eV, at  $x = 5$ , to 2.10 eV, at  $x = 40$  (Fig. 10, Table 2). Extrinsic absorption bands in infrared region originate from hydroxyl ions (near 3.06  $\mu\text{m}$ ), CO<sub>2</sub>

impurities (near 4.46  $\mu\text{m}$ ), and silicon-oxygen vibrations (near 5.6  $\mu\text{m}$ ) (Fig. 11). The last one is partially covered by multiphonon absorption edge. This edge takes place at 5.0 – 5.4  $\mu\text{m}$ .

#### 4. Discussion

As for  $x > 0$  the concentration of  $\text{Li}_2\text{O}$  is constant, the ionic component of the DC conductivity, due to movement of  $\text{Li}^+$  ions, does not change significantly with increasing concentration of  $\text{MoO}_3$ . However, degree of disorder increases with increasing concentration of  $\text{MoO}_3$  due to the creation of dangling bonds and non-bridging oxygens. It can result in the decrease of  $\text{Li}^+$  ions jump distance and in slight contribution to the increase of the ionic component of the conductivity with increasing  $\text{MoO}_3$  content [14]. The rapid, almost exponential increase of the electrical conductivity with increasing  $\text{MoO}_3$  content results most probably from the polaronic transfer between  $\text{Mo}^{5+}$  and  $\text{Mo}^{6+}$  ions [10, 12, 14, 23]. From the polaronic viewpoint, an electron delivered by Li atoms at the  $\text{Mo}^{6+}$  site converts this ion into a lower valence state  $\text{Mo}^{5+}$  and at the next step, the trapped electron at this  $\text{Mo}^{5+}$  site is transferred to the neighboring  $\text{Mo}^{6+}$  site by thermal or optical activation. This polaron hopping is a usual conduction mechanism of transitive metal ions in glasses because the disordered structure supports the polaron formation [23-26]. The idea of a polaron transfer in antimonite glasses containing  $\text{MoO}_3$  is supported by optical absorption measurements that show broadened polaron bands from polaronic transfer between  $\text{Mo}^{5+}$  and  $\text{Mo}^{6+}$  ions [10, 14]. The pre-exponential factor,  $\sigma_0$ , goes through a maximum,  $\sigma_0 = 1.7 \times 10^4$  S/m, at  $x = 25$  (Table 1). Its sharp peak occurs close to the composition of glasses with the highest  $T_g$  (289 °C) and the broadest thermal stability range ( $T_x - T_g = 153$  °C), at  $x = 20$  (Table 2). At the close  $\text{MoO}_3$  concentration,  $x = 25$ , there is a slight bend in the concentration dependence of the conduction activation energy,  $E_\sigma$ . It indicates the structural change close to this concentration, probably the development of  $[\text{MoO}_6]$  octahedrons on account of  $[\text{MoO}_4]$  tetrahedrons at increasing concentration of  $\text{MoO}_3$  [9, 10, 12-15].

In molybdenum-free glasses, the low-temperature part of the DC conductivity comes, probably, from the small polaron hopping between  $\text{Sb}^{3+}$  and  $\text{Sb}^{5+}$  ions at Fermi level [23, 26, 27]. At high temperatures, in the molybdenum-free glass, polarization effects next to electrodes limit the DC conductivity by  $\text{Li}^+$  ions at high conductivities. The conduction mechanism by  $\text{Li}^+$  ions dominates the conductivity over the main temperature range in this glass. However, as the quality of this glass is bad (Figs. 9, 11), also high

concentration of defects can result in the anomalous temperature dependence of the DC conductivity. The bad quality of this glass probably results from the absence of the glass forming ability and stabilizing activity of MoO<sub>3</sub> oxide in the antimonite glasses [1, 2]. Also the of optical edge analysis indicates the highest dynamic disorder in this glass [19].

The frequency dependence of the AC conductivity in glasses, in our frequency range, is usually composed of two parts: the DC bulk conductivity,  $\sigma(0)$ , and an AC component,  $\sigma_{\omega}$ , equal to  $Af^n$ , where  $f$  is the frequency in Hz:

$$\sigma_{AC}(f) = \sigma(0) + \sigma_{\omega} = \sigma(0) + Af^n. \quad (3)$$

The parameter  $A$  depends on the glass composition, temperature, and electrodes;  $n = 0.9 \pm 0.1$ , for homogeneous glasses [22, 23], and  $n = 0.5 \pm 0.1$ , for inhomogeneous glasses [24]. At this approximation, in SLM glasses, the value of  $n$  (0.6-1.1) decreases and the value of  $A$  increases with increasing DC conductivity or temperature. However, in our glasses, using this simple approximation, the value of  $\sigma(0)$  coincides with the value of DC conductivity,  $\sigma_{DC}$ , only at  $x \geq 20$  when the DC conductivity is sufficiently high. To receive a correct  $\sigma(0)$  and a better fit (higher regression coefficient) of the whole experimental frequency dependence it is necessary to suppose

$$\sigma_{AC}(f) = \sigma(0) + Af^n + Bf^m, \quad (2)$$

where  $n = 0.56-0.93$  and  $m \geq 1.6$  (Figs. 4, 5, Tables 3, 4). The third term,  $Bf^m$ , was already introduced earlier; it is supposed that it depends on the quality of electrode and sample surfaces [27-30]. The AC component of the conductivity,  $Af^n$ , is often explained by phonon-assisted pair-hopping mechanism at Fermi level [31]. It requires a decrease of  $n$  with increasing frequency,  $n \leq 0.85$ , and a linear temperature dependence of  $Af^n$ . This is not confirmed in our glasses. Elliott's model for hopping of bipolarons over a correlated barrier [32, 33] requires a temperature dependence of  $Af^n$ , what is observed because the parameter  $A$  increases with increasing temperature. However, it requires parameter  $n$  to be independent of temperature; still, in our glasses, this parameter decreases with increasing temperature (Table 4). Thus, Jonscher's universal model [34, 35] of dielectric response seems to be the most plausible explanation of our AC experiments.

A shape of modular diagrams,  $M''$  against  $M'$ , is regular for all our glasses. The diagrams are composed of slightly depressed circular arc and a high frequency linear tail as it is usual in semiconducting glasses (Fig. 6). From modular diagrams, we have calculated relative static permittivity,  $\epsilon_{rs}$ . Up to  $x = 10$ , the

permittivity decreases upon adding MoO<sub>3</sub>. At higher MoO<sub>3</sub> concentrations, the changes of the permittivity with an increasing MoO<sub>3</sub> concentration are not systematic (Table 2). For the permittivity, probably, not only the composition but also the defect concentration and homogeneity of the glass network is important.

Regular shape of modular spectra (Figs. 6, 7) confirms a single dominant conduction mechanism and relatively good ordering of glasses. The spectra are broadened comparing to Debye spectra and have a high-frequency tail as it is usual in glasses. Their maximums shift to higher frequencies with increasing DC conductivity of glasses; it means that they shift to higher frequencies also with increasing temperature. From the temperature dependences of the position of maximum of imaginary part of the modulus,  $M''$ , (Fig. 8) we have calculated the electrical relaxation time,  $\tau$ , and then the activation energy of electrical relaxation,  $E_\tau$ , from the relation

$$\tau = \tau_0 \exp(E_\tau/kT) \quad (4).$$

For  $x = 35$  and  $40$ , the activation energy of the electrical relaxation,  $E_\tau$ , is equal to  $0.954 \pm 0.008$  eV and the pre-exponential factor,  $\tau_0$ , is equal to  $(4.0 \pm 1.0) \cdot 10^{-14}$  s. This factor is in a good agreement with the frequency of molecular vibrations. The activation energy of electrical relaxation is close to the activation energy of the DC conductivity what indicates that both mechanisms are identical or very similar, at these concentrations of MoO<sub>3</sub>.

UV-visible absorption edge is ruled by the Urbach's tail (Fig. 9). This tail is directly related to the structural disordering of the glass network. Its width represents a measure of glass disordering [2]. In SLMx glasses [2], a dynamic disorder has the largest value in the MoO<sub>3</sub>-free glass; it has the smallest value at  $x = 30$ . In all glasses with  $x > 0$ , the conduction activation energy is close to the half of the indirect optical gap,  $E_\sigma/E_g = 0.45 \pm 0.01$  (Tables 1, 2).

Due to used technology of preparation, extrinsic absorption bands in infrared region originate from hydroxyl ions and CO<sub>2</sub> impurities due to a preparation in air, and silicon-oxygen vibrations due to a preparation in silica tubes.

## 5. Conclusions

Physical properties of lithium molybdenum-antimonite glasses,  $(80-x)\text{Sb}_2\text{O}_3\text{-}20\text{Li}_2\text{O-}x\text{MoO}_3$ ,  $x = 0 - 40$ , are measured and discussed.

UV-visible absorption edge shifts to lower energies and its slope decreases with increasing MoO<sub>3</sub> content; at the same time, the color of glasses changes from light yellow to dark brown.

Due to the preparation technology, absorption bands in infrared region originate from hydroxyl ions, CO<sub>2</sub> impurities, and silicon-oxygen vibrations.

With increasing MoO<sub>3</sub> content the density of glasses decreases. The glass transition temperature, the crystallization temperature, and the thermal stability range, go through their maximums at 20 – 25 mol % MoO<sub>3</sub>.

For  $x > 0$ , temperature dependences of the DC conductivity are Arrhenius-like. With increasing concentration of MoO<sub>3</sub> the dc conductivity exponentially increases and the conduction activation energy monotonously decreases. The conduction activation energy is close to a half of the optical gap ( $E_{\sigma}/E_g = 0.45 \pm 0.01$ ).

Regular shape of modular spectra and modular diagrams confirms a single dominant conduction mechanism and a good ordering of glasses. The maximums of modular spectra shift to higher frequencies with increasing DC conductivity or increasing temperature. The activation energy of electrical relaxation calculated from this shift is close to the conduction activation energy

Probably, near  $x = 25$ , a structural change occurs – the development of [MoO<sub>6</sub>] octahedrons takes place, all measured properties have anomalies at this concentration.

The paper brings new information on this glass system –

dependencies of important parameters on the concentration of MoO<sub>3</sub>;

broad thermal stability range indicating that glasses with 15-25 mole % MoO<sub>3</sub> are suitable for fiber drawing;

the conduction activation energy is close to a half of the optical gap what indicates a dominant contribution of Mo<sup>5+</sup>-Mo<sup>6+</sup> polaron pairs to the conductivity in MoO<sub>3</sub> containing glasses;

the conduction activation energy is close to the activation energy of electrical relaxation what indicates similar dominant mechanisms of electrical conduction and relaxation.

## **Acknowledgements**

This research was supported by the Slovak National Science Foundation APVV (projects No. SK-CZ-2013-0182 and SK-FR-2013-007), Scientific Grant Agency VEGA (projects No. 1/0184/14 and 1/0162/15), and Czech Science Foundation (project No. P106/12/2384).

## References

- [1] M.T. Soltani, T. Djouama, A. Boutarfaia, M. Poulain, New heavy metal oxide glasses based on  $\text{Sb}_2\text{O}_3$ , *J. Optoelect. Advanced Mater. Symp.* 1 (2009) 339-342.
- [2] M.T. Soltani, A. Boutarfaia, R. Makhloufi, M. Poulain, New alkali antimonate glasses, *J. Phys. Chem. Solids* 64 (2003) 2307-2312.
- [3] M. Baazouzi, M.T. Soltani, M. Hamzaoui, M. Poulain, J. Troles, Optical properties of alkali-antimonite glasses and purified processes for fiber drawing, *Opt. Mater.* 36 (2013) 500-504.
- [4] M. Nalin, M. Poulain, M. Poulain, S.J.L. Ribeiro, Y. Massaddeq, Antimony oxide based glasses, *J. Non Cryst. Solids* 284 (2001) 110-116.
- [5] A.E. Ersundu, M. Celikbilek, M. Baazouzi, M.T. Soltani, J. Troles, S. Aydin, Characterization of new  $\text{Sb}_2\text{O}_3$ -based multicomponent heavy metal oxide glasses, *J. Alloys Comp.* 615 (2014) 712-718.
- [6] C.B. de Araújo, G. Boudebs, V. Briois, A. Pradel, Y. Messaddeq, M. Nalin, Nonlinear refractive index measurements in antimony-sulfide glass films using a single beam nonlinear image technique, *Opt. Commun.* 260 (2006) 723-726.
- [7] T. Honma, R. Sato, Y. Benino, T. Komatsu, V. Dimitrov, Electronic polarizability, optical basicity and XPS spectra of  $\text{Sb}_2\text{O}_3$ - $\text{B}_2\text{O}_3$  glasses, *J. Non-Cryst. Solids* 272 (2000) 1-13.
- [8] M. Mee, B.C. Davis, R.G. Orman, M.F. Thomas, D. Holland, Antimony and silicon environments in antimony silicate glasses, *J. Solid State Chem.* 183 (2010) 1925-1934.
- [9] F. Goumeidane, M. Legouera, M. Iezid, M. Poulain, V. Nazabal, R. Lebullenger, Synthesis and physical properties of glasses in the  $\text{Sb}_2\text{O}_3$ - $\text{PbCl}_2$ - $\text{MoO}_3$  system, *J. Non-Cryst. Solids* 357 (2011) 3572-3577.
- [10] A. Padmanabham, V. Ravi Kumar, T. Satyanarayana, N. Veeraiah, Induced crystallization and the physical properties of  $\text{PbO}$ - $\text{Sb}_2\text{O}_3$ - $\text{As}_2\text{O}_3$ : $\text{MoO}_3$  glass system, *J. Phys. Chem. Solids* 70 (2009) 669-679.
- [11] T. Som, B. Karmakar, Structure and properties of low-phonon antimony glasses and nano glass-ceramics in  $\text{K}_2\text{O}$ - $\text{B}_2\text{O}_3$ - $\text{Sb}_2\text{O}_3$  system, *J. Non-Cryst. Solids* 356 (2010) 1925-1934.

- [12] S. BalaMuraliKrishna, A. Ramesh Babu, Ch. RajyaSree, D. Krishna Rao, Influence of molybdenum ions on the structure of ZnO-As<sub>2</sub>O<sub>3</sub>-Sb<sub>2</sub>O<sub>3</sub> glass system by means of spectroscopic and dielectric studies, *J. Non-Cryst. Solids* 536 (2010) 1754-1761.
- [13] G. Little Flower, G. Sahara Baskaran, M. Srinivasa Reddy, N. Veeraiah, The structural investigations of PbO-P<sub>2</sub>O<sub>5</sub>-Sb<sub>2</sub>O<sub>3</sub> glasses with MoO<sub>3</sub> as additive by means of dielectric, spectroscopic and magnetic studies, *Physica B* 393 (2007) 61-72.
- [14] R. Vijay, P. Ramesh-Babu, Y. Gandhi, M. Piasecki, D. Krishna Rao, N. Veeraiah, Molybdenum ion: a structural probe in lithium-antimony-germanate glass system by means of dielectric and spectroscopic studies, *J. Mater. Sci.* (2014) DOI 10.1007/s10853-014-8345-6
- [15] P. Naresh, G. Naga Raju, M. Srinivas Reddy, T. Venkatappa Rao, I.V.Kityk, N. Veeraiah, Dielectric and spectroscopic features of ZnO-ZnF<sub>2</sub>-B<sub>2</sub>O<sub>3</sub>:MoO<sub>3</sub> glass ceramic – a possible material for plasma display panels, *J. Mater. Sci.:Mater. Electron.* (2014) DOI 10.1007/s10854-014-2251-1.
- [16] V. Labaš, M.Poulain, M.Kubliha, V. Trnvcová, F. Goumeidane, Electrical, dielectric and optical properties of Sb<sub>2</sub>O<sub>3</sub>-PbCl<sub>2</sub>-MoO<sub>3</sub> glasses, *J. Non-Cryst. Solids* 377 (2013) 66-69.
- [17] J. Kalužný, M. Poulain, M. Kubliha, V. Adamčík, M. Legouera, T. Soltani, E. Mariani, Electrical, dielectrical and optical properties of glasses based on Sb<sub>2</sub>O<sub>3</sub>, *Proceedings of 13th International Symposium ISNOG: Extended Abstracts. Part 1.* Pardubice:University Pardubice, 2002, p. 276-279.
- [18] M. Kubliha, Investigating structural changes and defects of non-metallic materials via electrical methods, Dresden: Forschungszentrum, Dresden–Rossendorf2009.
- [19] P. Petkova, H. Touiri, M.T. Soltani, Investigation of Urbach's rule region in undoped and Cu doped (80-x) Sb<sub>2</sub>O<sub>3</sub>-20Li<sub>2</sub>O-xMoO<sub>3</sub> glasses, *Phys. Scr.* T157 (2013) 014041 (4pp).
- [20] M.T. Soltani, M. Hamzaoui, S. Houhou, H. Touiri, L. Bediar A.M. Ghemri. P. Petkova, Physical characterization of Sb<sub>2</sub>O<sub>3</sub>-M<sub>2</sub>O-MoO<sub>3</sub>(M = Li, K) new glasses, *Acta Phys. Polonica A* 123 (2013) 227-229.
- [21] I. Štubňa, V. Trnvcová, L. Vozár, S. Csáki, Uncertainty of the measurement of the DC conductivity of ceramics at elevated temperatures, *J. Electr. Eng.* 66 (2015) 34-39.
- [22] P.B. Macedo, C.T. Moynihan, R. Bose, *Phys. Chem. Glasses* 13 (1972) 171-176.
- [23] I. Oliva, A. Masuno, H. Inoue, M. Sakamoto, K. Morita, Adiabatic small polaron hopping in K<sub>2</sub>O-WO<sub>3</sub>-Nb<sub>2</sub>O<sub>5</sub>-P<sub>2</sub>O<sub>5</sub> glasses, *Solid State Ionics* 255 (2014) 56-59.

- [24] C. Cramer, K. Funke, B. Roling, T. Saatkamp, D. Wilmer, M.D. Ingram, A. Pradel, M. Ribes, G. Taillades, Ionic and polaronic hopping in glass, *Solid State Ionics* 86 (1996) 481-486.
- [25] S.R. Elliott, *Physics of amorphous materials*, *Adv. Phys* 36 (1987) 135-170.
- [26] I.G. Austin, N.F. Mott, Polarons in crystalline and non-crystalline materials, *Adv. Phys.* 18 (1969) 41-102
- [27] N.F. Mott, E.A. Davis, *Electronic processes in non-crystalline materials*, Oxford University Press, Oxford 1974.
- [28] V. Trnovcová, I. Furár, D. Ležal, Influence of doping on physical properties of vitreous  $\text{As}_2\text{Se}_3$ , *J. Non-Cryst. Solids*, 353 (2007) 1311-1314.
- [29] V. Trnovcová, I. Furár, Electrical and dielectric properties of As-Se glasses with uranium, *J. Opt. & Advanced Mater.*, 11 (2009) 2058-2062.
- [30] S.R. Elliott, On the super-linear frequency dependent conductivity of amorphous semiconductors, *Solid State Comm.* 28 (1978) 939-942.
- [31] M. Pollak, *Phil. Mag.*, 23 (1971) 519.
- [32] S.R. Elliott, *Phil. Mag.*, 36 (1977) 1291.
- [33] S.R. Elliott, *Phil. Mag.*, 37 (1978) 135.
- [34] A.K. Jonscher, *Dielectric relaxation in solids*, Chelsea Dielectrics Press, London 1983.
- [35] J. Ross MacDonald, Possible universalities in the ac frequency response of dispersed, disordered materials, *J. Non-Cryst. Solids* 210 (1997) 70-86.

## Figure captions:

Figure 1. DSC diagrams of  $(80-x)\text{Sb}_2\text{O}_3-20\text{Li}_2\text{O}-x\text{MoO}_3$ , SLM $x$ , glasses.

Figure 2. Temperature dependencies of the DC conductivity of  $(80-x)\text{Sb}_2\text{O}_3-20\text{Li}_2\text{O}-x\text{MoO}_3$ , SLM $x$ , glasses (error bars of all dependencies are indicated in the left bottom corner of the figure).

Figure 3. Concentration dependence of the DC conductivity,  $\sigma_{\text{DC}}$ , at 150 °C, for  $(80-x)\text{Sb}_2\text{O}_3-20\text{Li}_2\text{O}-x\text{MoO}_3$ , SLM $x$ , glasses (error bars of all dependencies are indicated in the left bottom corner of the figure).

Figure 4. Frequency dependencies of the AC conductivity of  $(80-x)\text{Sb}_2\text{O}_3-20\text{Li}_2\text{O}-x\text{MoO}_3$ , SLM $x$ , glasses, at 200°C, approximated as  $\sigma_{\text{AC}}(f) = \sigma(0) + A f^n + B f^m$  (error bars of all dependencies are indicated in the right bottom corner of the figure) .

Figure 5. Frequency dependencies of the AC conductivity of  $55\text{Sb}_2\text{O}_3-20\text{Li}_2\text{O}-25\text{MoO}_3$  glass, at various temperatures, approximated as  $\sigma_{\text{AC}}(f) = \sigma(0) + A f^n + B f^m$  (error bars of all dependencies are indicated in the right bottom corner of the figure).

Figure 6. Modular diagrams of  $(80-x)\text{Sb}_2\text{O}_3-20\text{Li}_2\text{O}-x\text{MoO}_3$ , SLM $x$ , glasses at 200 °C (error bars of all dependencies are indicated in the left bottom corner of the figure).

Figure 7. Modular spectra of  $(80-x)\text{Sb}_2\text{O}_3-20\text{Li}_2\text{O}-x\text{MoO}_3$ , SLM $x$ , glasses at 200 °C (error bars of all dependencies are indicated in the upper part of the figure).

Figure 8. Modular spectra of  $40\text{Sb}_2\text{O}_3-20\text{Li}_2\text{O}-40\text{MoO}_3$  glass, at various temperatures (error bars of all dependencies are indicated in the upper part of the figure).

Figure 9. UV/VIS absorption edge of  $(80-x)\text{Sb}_2\text{O}_3-20\text{Li}_2\text{O}-x\text{MoO}_3$ , SLM $x$ , glasses (error bars are smaller than the size of experimental points).

Figure 10. Tauc plots of  $(80-x)\text{Sb}_2\text{O}_3-20\text{Li}_2\text{O}-x\text{MoO}_3$ , SLM $x$ , glasses, at  $x \geq 5$  (error bars are smaller than the size of experimental points).

Figure 11. Infrared spectra of  $(80-x)\text{Sb}_2\text{O}_3-20\text{Li}_2\text{O}-x\text{MoO}_3$ , SLM $x$ , glasses.

**Table captions:**

Table 1.

Compositions, colors, DC conduction activation energies,  $E_{\sigma}$ , pre-exponential factors,  $\sigma_0$ , and corresponding correlation coefficients,  $r$ , of  $(80 - x)\text{Sb}_2\text{O}_3\text{-}20\text{Li}_2\text{O-xMoO}_3$ , SLMx, glasses.

	$\text{Sb}_2\text{O}_3$ [mol%]	$\text{Li}_2\text{O}$ [mol%]	$\text{MoO}_3$ [mol%]	Color	$E_{\sigma}$ (main temperature ranges) [eV]	$\sigma_0$ [S/m]	$r$
SLM00 80	80	20	0		$0.78 \pm 0.09$ (194–220 °C) $1.161 \pm 0.003$ (125–170 °C) $0.48 \pm 0.04$ (40– 100 °C)	$(5.11 \pm 0.02) \times 10^{-4}$ $(5.9 \pm 0.5) \times 10^3$ $(8.7 \pm 0.9) \times 10^{-6}$	$-0.99978$ $-0.99697$ $-0.9967$
SLM05 75	75	20	5		$1.151 \pm 0.003$ (110–220 °C)	$(2.9 \pm 0.1) \times 10^3$	$-0.99974$
SLM10 70	70	20	10		$1.136 \pm 0.002$ (110–220 °C)	$(5.3 \pm 0.2) \times 10^3$	$-0.99989$
SLM15 65	65	20	15		$1.108 \pm 0.001$ (85–220 °C)	$(6.9 \pm 0.2) \times 10^3$	$-0.99993$
SLM20 60	60	20	20		$1.092 \pm 0.001$ (95–220 °C)	$(1.35 \pm 0.01) \times 10^4$	$-0.99999$
SLM25 55	55	20	25		$1.069 \pm 0.001$ (80–220 °C)	$(1.69 \pm 0.02) \times 10^4$	$-0.99997$
SLM30 50	50	20	30		$1.016 \pm 0.001$ (80–220 °C)	$(7.5 \pm 0.1) \times 10^3$	$-0.99996$
SLM35 45	45	20	35		$0.962 \pm 0.001$ (40–210 °C)	$(3.8 \pm 0.05) \times 10^3$	$-0.99996$
SLM40 40	40	20	40		$0.914 \pm 0.001$ (55–205 °C)	$(2.68 \pm 0.04) \times 10^3$	$-0.99996$

Table 2.

Glass transition temperature,  $T_g$ , temperature of crystallization,  $T_x$ , thermal stability range,  $T_x - T_g$ , density,  $d$ , relative static permittivity,  $\epsilon_{rs}$ , and indirect optical gap,  $E_g$ , with corresponding correlation coefficients,  $r$ , of SLMx glasses.

	$T_g$ [°C]	$T_x$ [°C]	$T_x - T_g$ [°C]	$d$ [g/cm <sup>3</sup> ]	$\epsilon_{rs}$	$r_\epsilon$	$E_g$ [eV]	$r_E$
SLM00	273	385	112	4.916	$19.5 \pm 0.3$	$-0.95815$		
SLM05	277	405	128		$18.7 \pm 0.3$	$-0.98544$	$2.57 \pm 0.05$	0.99895
SLM10	281	409	128	4.783	$17.4 \pm 0.2$	$-0.99181$	$2.52 \pm 0.05$	0.99943
SLM15	288	433	145		$19.9 \pm 0.2$	$-0.99696$	$2.48 \pm 0.05$	0.99943
SLM20	289	442	153	4.701	$19.2 \pm 0.2$	$-0.99826$	$2.42 \pm 0.04$	0.99944
SLM25	281	423	142		$21.3 \pm 0.2$	$-0.9982$	$2.36 \pm 0.03$	0.9997
SLM30	274	403	129	4.572	$17.4 \pm 0.2$	$-0.99839$	$2.26 \pm 0.03$	0.99982
SLM35	268	396	128		$23.0 \pm 0.2$	$-0.99877$	$2.20 \pm 0.04$	0.99951
SLM40	259	378	119	4.438	$22.2 \pm 0.2$	$-0.99898$	$2.10 \pm 0.02$	0.99987

Table 3.

Parameters of frequency dependencies of the AC conductivity,  $\sigma_{AC}(f) = \sigma(0) + A f^n + B f^m$ , and corresponding correlation coefficients,  $r$ , of SLMx glasses at 200 °C.

	$A$ [S·m <sup>-1</sup> ]	$n$	$B$ [S·m <sup>-1</sup> ]	$m$	$\sigma(0)$ [S·m <sup>-1</sup> ]	$r$
SLM0 0	$(10 \pm 2) \times 10^{-12}$	$0.93 \pm 0.0$ 1	$(3.6 \pm 0.2) \times 10^{-3}$ 0	$4.5 \pm 0.$ 4	$(4.4 \pm 0.6) \times 10^{-9}$	0.9991
SLM0 5	$(2.9 \pm 0.6) \times 10^{-1}$ 1	$0.84 \pm 0.0$ 2	$(1.1 \pm 0.2) \times 10^{-2}$ 0	$2.6 \pm 0.$ 1	$(3.3 \pm 0.6) \times 10^{-9}$	0.9999 6
SLM1 0	$(3.9 \pm 0.7) \times 10^{-1}$ 1	$0.83 \pm 0.0$ 2	$(2.4 \pm 0.8) \times 10^{-2}$ 3	$3.2 \pm 0.$ 3	$(1.0 \pm 0.1) \times 10^{-8}$	0.9991
SLM1 5	$(1.7 \pm 0.2) \times 10^{-1}$ 0	$0.73 \pm 0.0$ 1	$(3.9 \pm 0.4) \times 10^{-2}$ 4	$3.3 \pm 0.$ 1	$(1.9 \pm 0.3) \times 10^{-8}$	0.9998 8
SLM2 0	$(7.5 \pm 0.2) \times 10^{-1}$ 0	$0.62 \pm 0.0$ 1	$(1.5 \pm 0.2) \times 10^{-1}$ 7	$2.1 \pm 0.$ 1	$(2.9 \pm 0.2) \times 10^{-8}$	0.9999 5
SLM2 5	$(1.9 \pm 0.2) \times 10^{-9}$	$0.56 \pm 0.0$ 1	$(3.7 \pm 0.4) \times 10^{-1}$ 6	$1.8 \pm 0.$ 1	$(5.5 \pm 0.2) \times 10^{-8}$	0.9999 7
SLM3 0	$(2.8 \pm 0.2) \times 10^{-9}$	$0.55 \pm 0.0$ 1	$(6.5 \pm 0.6) \times 10^{-1}$ 5	$1.6 \pm 0.$ 1	$(8.4 \pm 0.2) \times 10^{-8}$	0.9999 9
SLM3 5	$(4.6 \pm 0.3) \times 10^{-9}$	$0.56 \pm 0.0$ 1	$(3.3 \pm 0.8) \times 10^{-1}$ 7	$2.0 \pm 0.$ 2	$(2.1 \pm 0.3) \times 10^{-7}$	0.9999 8
SLM4 0	$(5.2 \pm 0.2) \times 10^{-9}$	$0.59 \pm 0.0$ 1	$(6.2 \pm 0.4) \times 10^{-2}$ 8	$4.1 \pm 0.$ 5	$(5.2 \pm 0.4) \times 10^{-7}$	0.9997

Table 4.

Parameters of frequency dependencies of the AC conductivity,  $\sigma_{AC}(f) = \sigma(0) + A f^n + B f^m$ , and corresponding correlation coefficients,  $r$ , of SLM25 glass at different temperatures.

$T$ [°C]	$A$ [S·m <sup>-1</sup> ]	$n$	$B$ [S·m <sup>-1</sup> ]	$m$	$\sigma(0)$ [S·m <sup>-1</sup> ]	$r$
150	$(5.1 \pm 0.7) \times 10^{-11}$	$0.83 \pm 0.01$	$(1.0 \pm 0.4) \times 10^{-27}$	$4.0 \pm 0.3$	$(1.0 \pm 0.1) \times 10^{-8}$	0.9999
160	$(1.3 \pm 0.2) \times 10^{-10}$	$0.75 \pm 0.01$	$(5 \pm 1) \times 10^{-21}$	$2.7 \pm 0.2$	$(1.3 \pm 0.1) \times 10^{-8}$	0.99993
170	$(2.0 \pm 0.2) \times 10^{-10}$	$0.73 \pm 0.01$	$(5 \pm 1) \times 10^{-23}$	$3.1 \pm 0.2$	$(1.9 \pm 0.2) \times 10^{-8}$	0.99994
180	$(4.0 \pm 0.5) \times 10^{-10}$	$0.68 \pm 0.01$	$(7 \pm 2) \times 10^{-21}$	$2.7 \pm 0.2$	$(2.7 \pm 0.2) \times 10^{-8}$	0.99992
190	$(8.6 \pm 0.8) \times 10^{-10}$	$0.63 \pm 0.01$	$(4.4 \pm 0.9) \times 10^{-21}$	$2.8 \pm 0.2$	$(3.8 \pm 0.2) \times 10^{-8}$	0.99994
200	$(1.9 \pm 0.2) \times 10^{-9}$	$0.56 \pm 0.01$	$(3.7 \pm 0.4) \times 10^{-16}$	$1.8 \pm 0.1$	$(5.5 \pm 0.2) \times 10^{-8}$	0.99998

Table 5.

Electrical relaxation times,  $\tau$ , their relaxation activation energies,  $E_\tau$ , pre-exponential factors,  $\tau_0$ , and corresponding correlation coefficients,  $r$ , of SLM30, SLM35, and SLM40 glasses.

	$T$ [°C]	$10^3 \times \tau$ [s <sup>-1</sup> ]	$E_\tau$ [eV]	$10^{14} \times \tau_0$ [s <sup>-1</sup> ]
SLM 30	200	$1.570 \pm 0.004$		
SLM 35	190	$1.509 \pm 0.004$	$0.96 \pm 0.06$	$5 \pm 3$
	200	$0.905 \pm 0.003$		
	170	$1.639 \pm 0.004$		
SLM 40	180	$0.972 \pm 0.002$	$0.95 \pm 0.03$	$3 \pm 1$
	190	$0.558 \pm 0.002$		
	200	$0.343 \pm 0.001$		

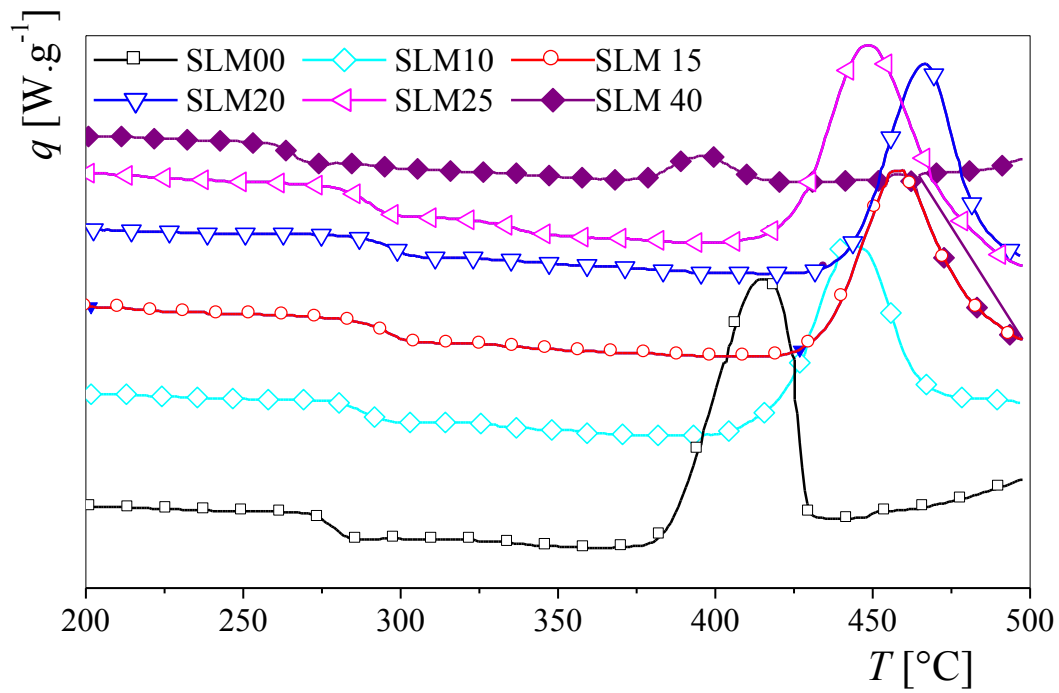


Fig. 1.

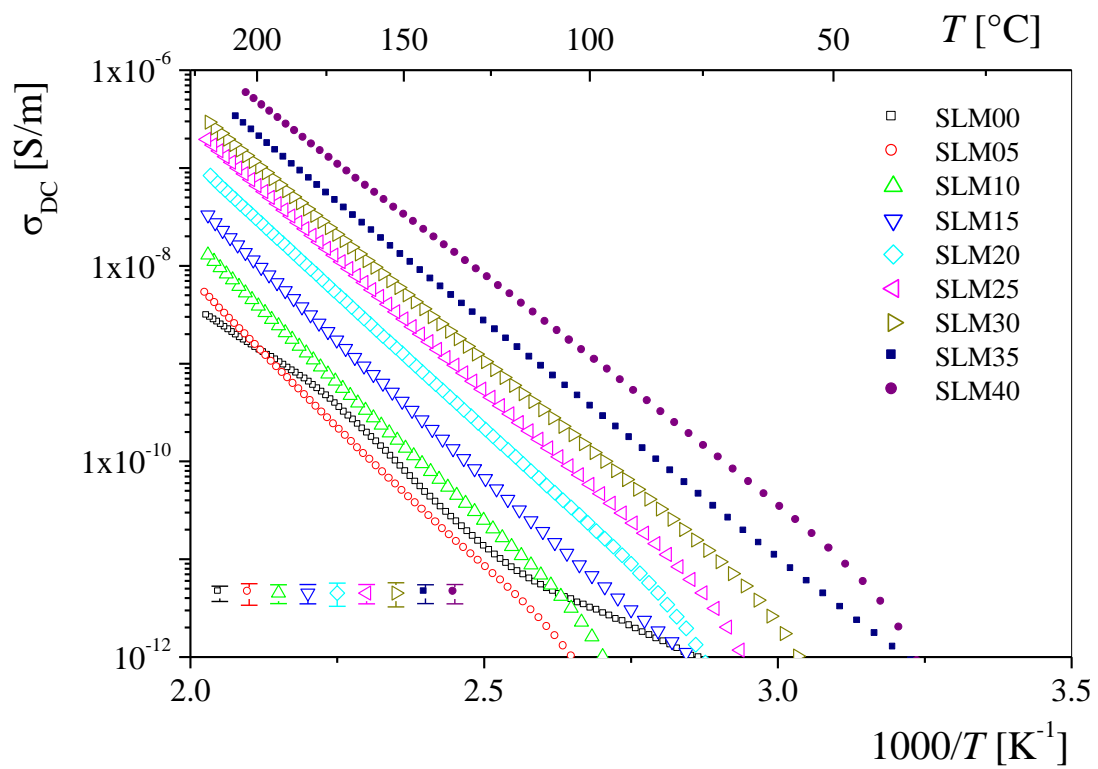


Fig. 2.

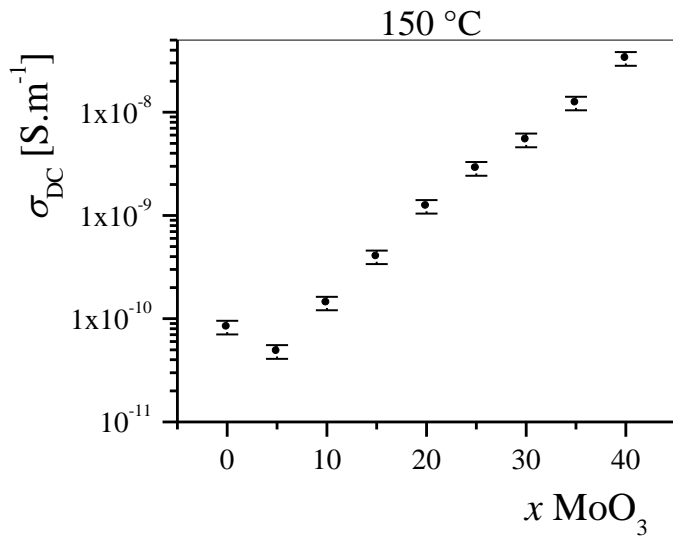


Fig. 3.

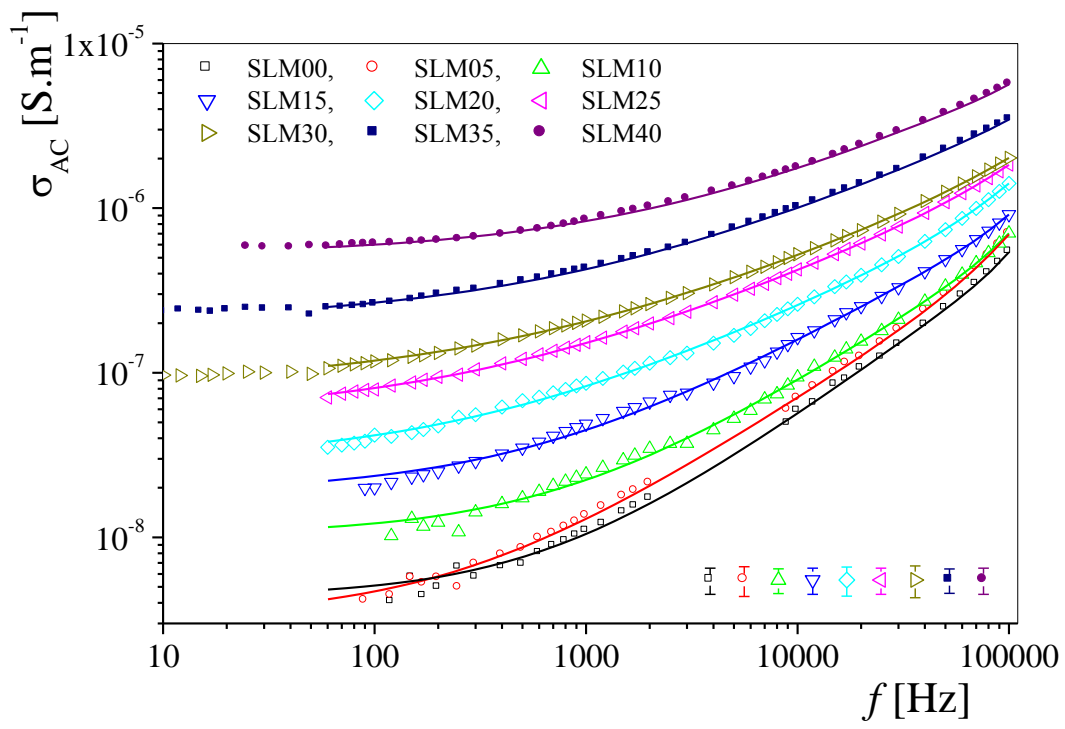


Fig. 4.

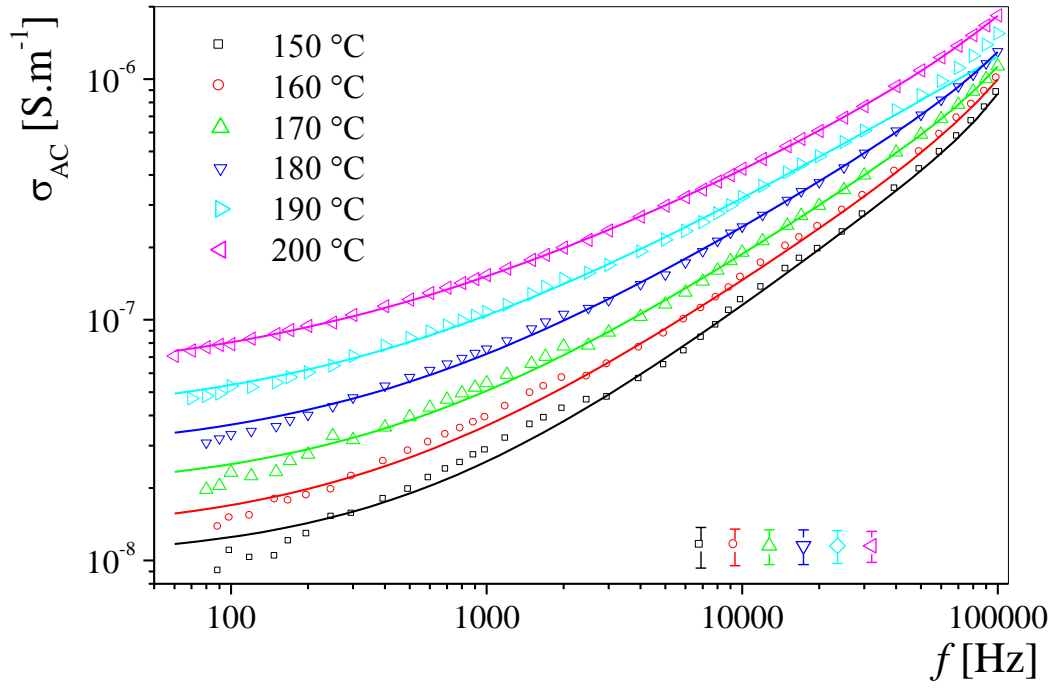


Fig. 5.

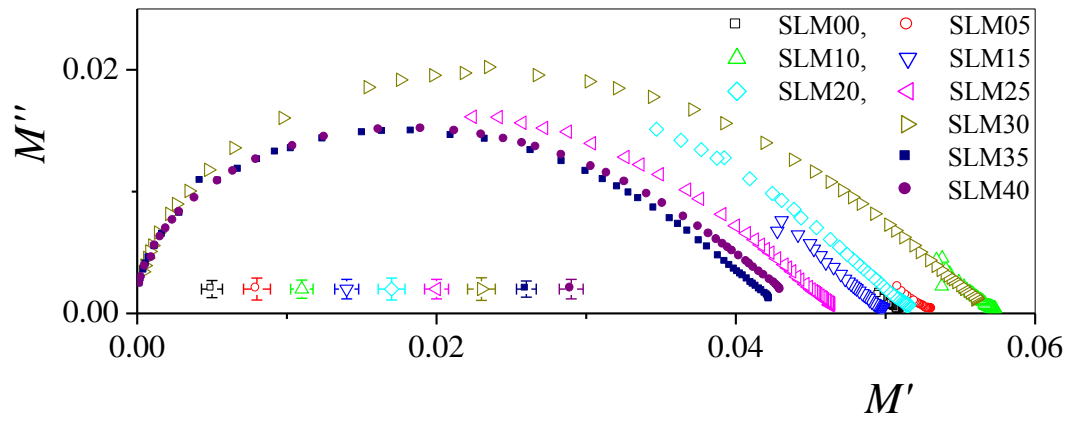


Fig. 6.

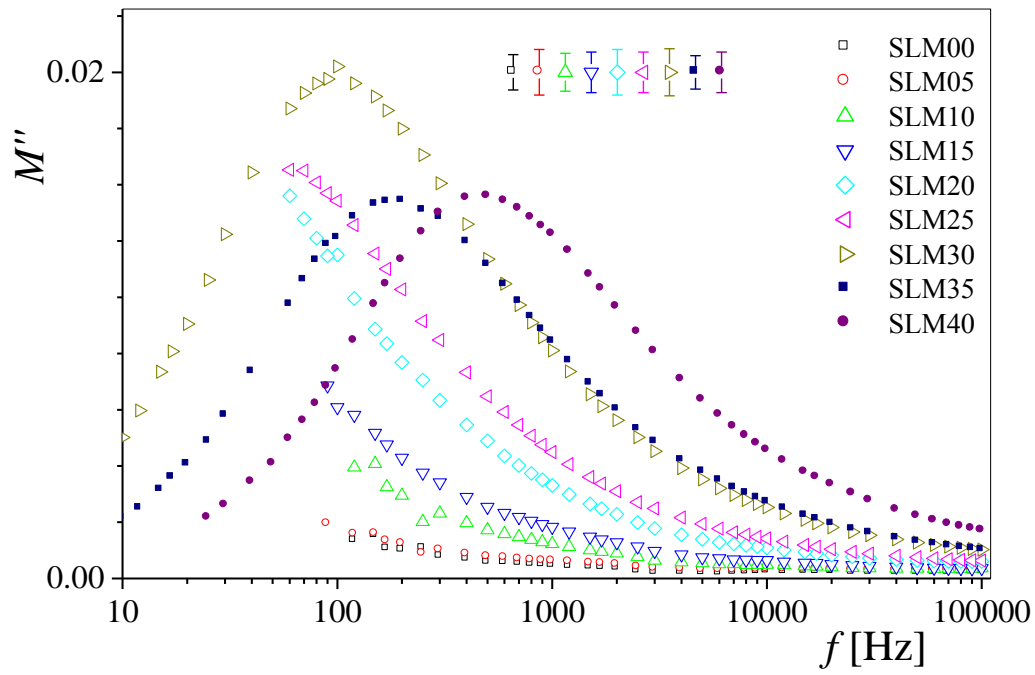


Fig. 7.

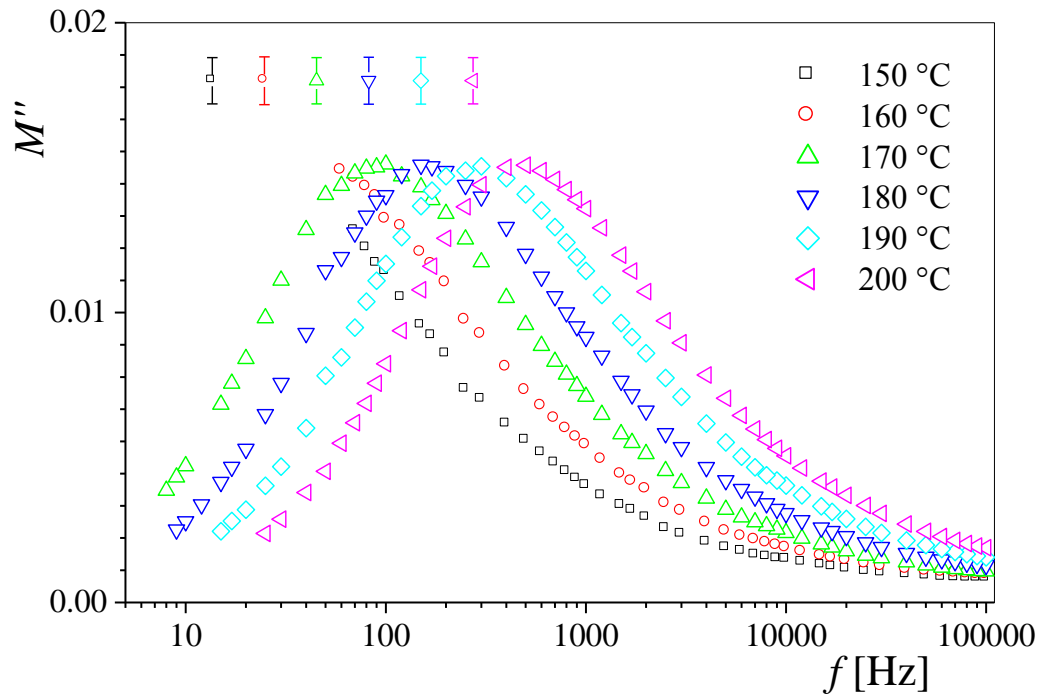


Fig. 8.

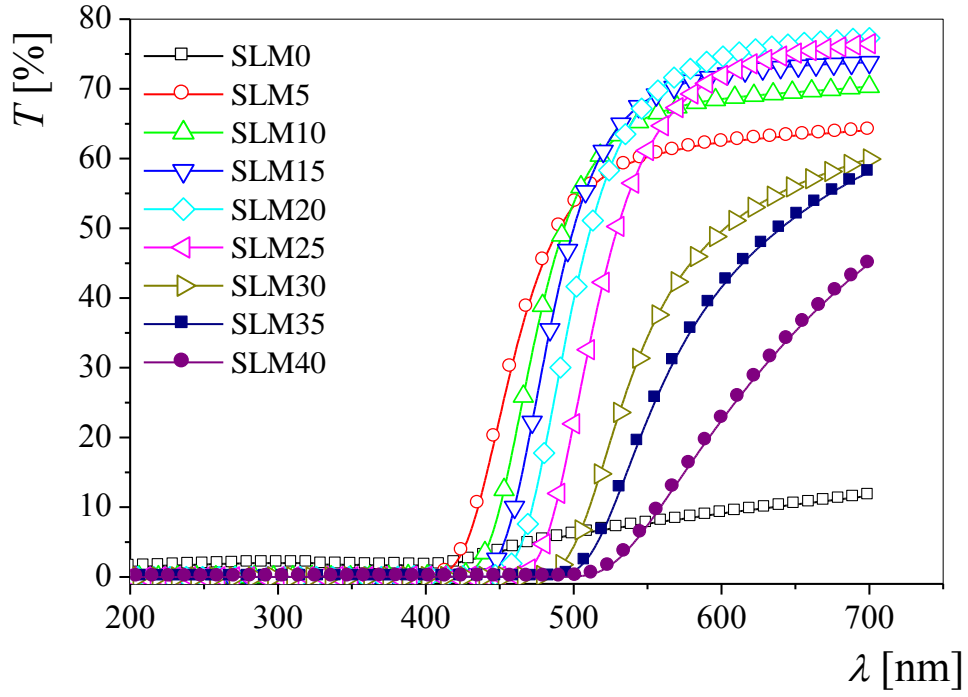


Fig. 9.

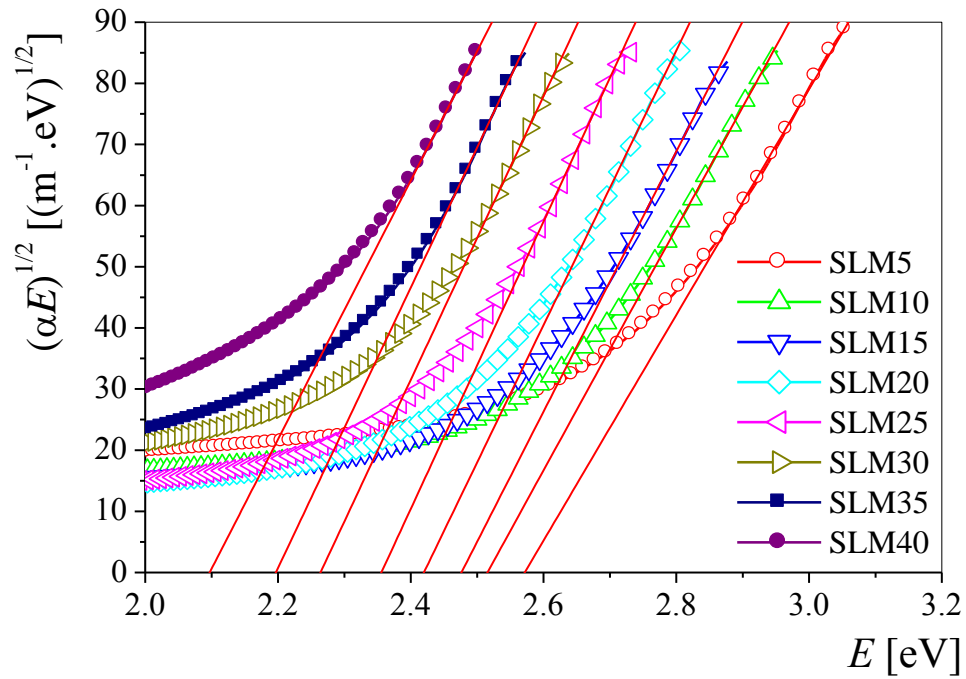


Fig. 10.

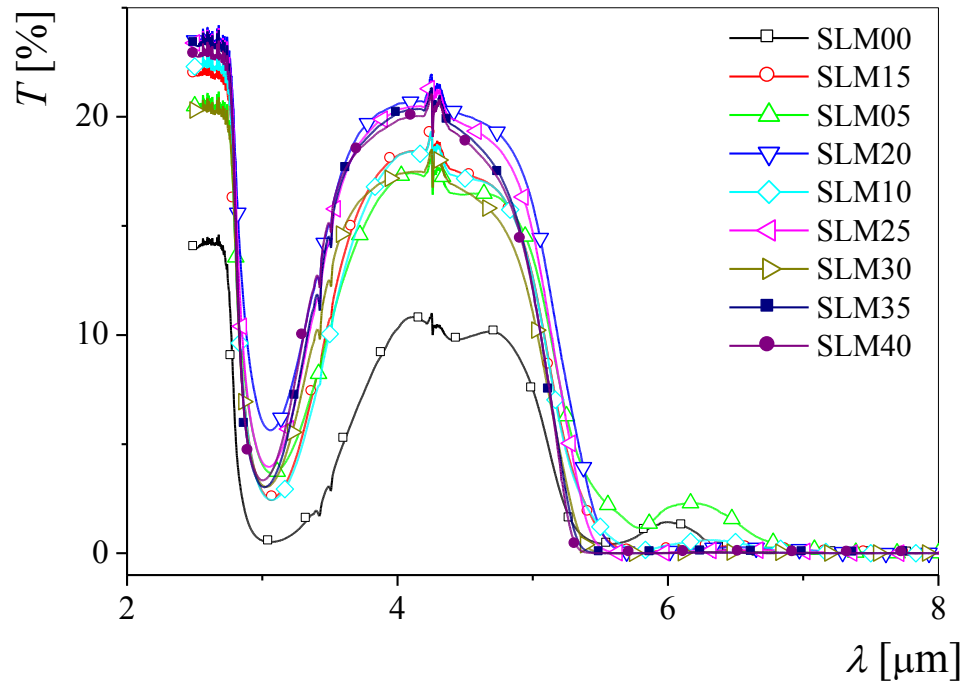


Fig. 11.